VSG Multi-Machine Parallel Power Decoupling Strategy Based on Improved Virtual Impedance

Yu Gao, Yin-Qing Wang, Xiao-Long Kong, Fei Guo, Yao-Yang Jin, and Meng-Yuan Xue

***Abstract*—Under low-voltage microgrid conditions, when virtual synchronous generators (VSG) are connected in parallel with loads, there is power coupling between the output active and reactive power due to the resistive characteristic of the equivalent transmission impedance, and the output power suppression effect cannot be accurately distributed with poor current circulation, which seriously affects the steady-state performance of the system; Secondly, the line impedance of each inverter control system often does not match the capacity ratio, making the traditional virtual impedance decoupling strategy somewhat limited. The paper proposes a power decoupling strategy based on improved virtual impedance to address this problem by using a fuzzy algorithm to monitor the VSG power angle to adjust the virtual impedance in real time and still meet the requirements of VSG parallel operation power equalization and circulating current suppression during sudden load changes. Finally, a VSG simulation model is constructed in MATLAB/Simulink to verify the feasibility of the proposed method.**

***Index Terms*—Fuzzy control, Power decoupling, Power distribution, Virtual synchronous generator, Virtual impedance**

I. Introduction

As the application of distributed generation (DG) supply becomes more and more widespread, the inverter becomes particularly important as the AC-DC converter interface, whose response speed and load limit determine the stability of the microgrid system, and the inverter control strategy becomes especially important. Compared to the conventional control strategy, the virtual synchronous generator (VSG) control technique provides damping and virtual inertia to the system by simulating the characteristics of the synchronous generator based on the original droop control [1]. In islanding mode, the system usually operates in parallel with VSGs, whose micro-sources and loads can be put in or removed on demand to enhance the redundancy and reliability of the system [2]-[3]. However, in the low-voltage microgrid environment, due to the resistive-inductive characteristics of the equivalent transmission impedance and the difference in line impedance, there is a coupling effect between active and reactive power, and the actual power distribution will deviate from the preset effect, generating current circulation between systems and affecting the stable operation of the parallel system [4]-[7].

The reference [8] uses droop control to adjust the equivalent internal resistance by constructing an adaptive virtual impedance to achieve the purpose of reducing the power error caused by the line impedance and improving the system stability, but the droop control algorithm is less robust and its parallel operation quality is inferior to that of the VSG algorithm. Reference [9] proposes an adaptive virtual impedance algorithm for the accurate calculation of line impedance by turning the power line into an equivalent circuit and then deriving a general solution for the line impedance from the internal voltage vector relationship, but there are too many uncertainties and variables in the complex line, which can lead to certain errors in practical application. Reference [10] identifies the line impedance by the short-time impulse response method and calculates the PCC endpoint voltage for voltage compensation, but the PCC endpoint voltage is an approximation of the sum of the inverter output voltage and the line impedance voltage drop, which also has error problems. Reference [11] uses a multi-intelligence coherence algorithm to adjust the virtual impedance value, cooperatively controls multiple VSGs, interconnects the power distribution information between the VSGs with an auxiliary controller, and then corrects it with the virtual impedance, but the control system is relatively complex and has the drawback of communication delay. In references [12]-[13], a virtual capacitor control algorithm is proposed by simulating the characteristics of the shunt capacitor at the output of the VSG, which reduces the steady-state reactive power distribution error but decreases the system stability. Reference [14] mixed VSG control with a fuzzy secondary controller (FSC) to measure the current at the PCC end, establish the mathematical equations to calculate the virtual impedance fitting the surface, and store the calculated virtual resistance values using a two-dimensional look-up table for online control, but the method requires a large amount of experimental data as a basis.

For the problem of uneven power distribution in VSG

Manuscript received March 18, 2023; revised July 17 2023.

Yu Gao is a postgraduate tutor in the Department of Electrical and Control Engineering at Xi'an University of Science and Technology, Xi'an, 710699, China. (e-mail: xkdgy@163.com).

Yin-Qing Wang is a postgraduate student in the Department of Electrical and Control Engineering at Xi'an University of Science and Technology, Xi'an, 710699, China. (e-mail: 1048196372@qq.com).

Xiao-Long Kong is a postgraduate student in the Department of Electrical and Control Engineering at Xi'an University of Science and Technology, Xi'an, 710699, China. (e-mail: 2690534666@qq.com).

Fei Guo is a postgraduate student in the Department of Electrical and Control Engineering at Xi'an University of Science and Technology, Xi'an, 710699, China. (e-mail: 3056883499@qq.com).

Yao-Yang Jin is a postgraduate student in the Department of Electrical and Control Engineering at Xi'an University of Science and Technology, Xi'an, 710699, China. (e-mail: 372312134@qq.com).

Meng-Yuan Xue is a postgraduate student in the Department of Electrical and Control Engineering at Xi'an University of Science and Technology, Xi'an, 710699, China. (e-mail: 1078012964@qq.com).

parallel systems operating with load, an improved virtual impedance decoupling strategy is proposed after analyzing the coupling mechanism. By using a fuzzy algorithm to find the non-linear relationship between power fluctuations and the amount of power angle variation, the VSG power angle is monitored, and thus the virtual impedance is adjusted in real time to mitigate the difference in line impedance at the inverter output, making the equivalent transmission impedance inductive, eliminating the coupling between powers, and limiting the current circulation. Finally, experiments were conducted to test the effectiveness of the suggested approach by creating models through a MATLAB/Simulink simulation system.

II. Basic Principle of VSG

VSG control introduces synchronous generator (SG) stator and rotor equations into the inverter algorithm, simulating the ontological characteristics of SG frequency and voltage modulation and inertial damping, making VSG have the dual advantages of the inverter and SG. The control block diagram of the two-inverter parallel system is shown in Fig. 1, where U_{dc} is the DC supply, L_f is the filter inductor, C_f is the filter capacitor, Z_{l1} is the line impedance, Z_L is the common load, i_{Labc} is the inductor side current, i_{abc} and u_{abc} are the output current and voltage, respectively, and $u_{abc\text{-}ref}$ is the reference voltage.

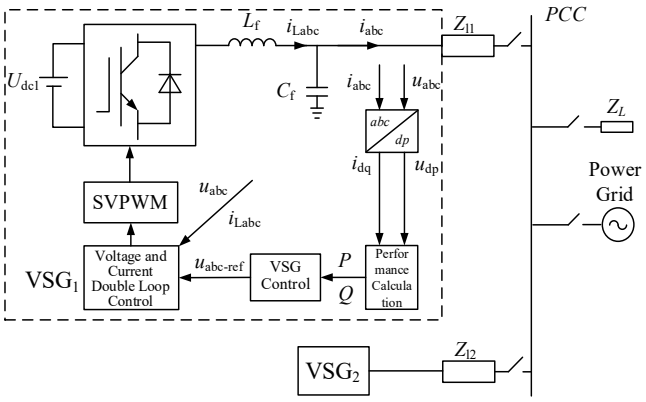

Fig. 1. Parallel control block diagram of VSG

The rotor mechanical equations construct the active power-frequency and reactive power-voltage loops of the VSG by means of a droop relationship with the following expressions:

$$\begin{cases} J\dfrac{d\omega}{dt} = T_m - T_e - T_D = \dfrac{P_m}{\omega_o} - \dfrac{P_e}{\omega_o} - D(\omega - \omega_o) \\ \dfrac{d\delta}{dt} = \omega - \omega_o \end{cases} \tag{1}$$

$$\begin{cases} P_m - P_{ref} = K_\omega(\omega_o - \omega) \\ E = E_{ref} + K_q(Q_{ref} - Q) \end{cases} \tag{2}$$

Where: J is the moment of inertia; T_m is the mechanical torque, T_e is the electromagnetic torque, D is the damping coefficient, ω is the actual angular velocity, ω_o is the reference angular velocity, δ is the output phase angle, P_m is the mechanical power, P_e is the electromagnetic power, P_{ref} is the VSG reference active power, K_ω is the active power-frequency modulation coefficient, K_q is the reactive power-voltage regulation coefficient, E is the VSG excitation electromotive force, E_{ref} is the rated electromotive force, Q_{ref} is the VSG reference reactive power, Q is the VSG output reactive power.

Figs. 2 and 3 are the active and reactive power loop control block diagrams of VSG.

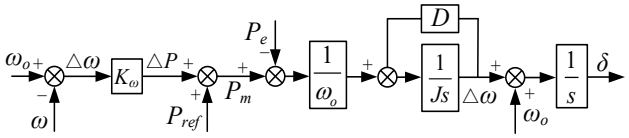

Fig. 2. Active power-frequency control block diagram

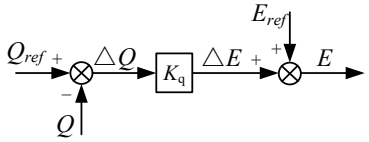

Fig. 3. Reactive power-voltage control block diagram

In the VSG control algorithm, the VSG output voltage and current are first measured, and the collected voltage and current are Park transformed to obtain the actual output active and reactive power by power calculation, and then delivered to the VSG control module, where the reference angle δ and reference electric potential E are obtained from the VSG active and reactive power loops. δ and E are voltage synthesized to obtain the three-phase voltage reference U_{ref}, and compared with the actual inverter output voltage and current for voltage-current dual closed loop control, and finally modulated by SVPWM.

III. Analysis of Parallel Characteristics of VSG

A. VSG parallel operation structure

Fig. 4 shows the equivalent circuit diagram of a VSG twin parallel system with load under islanding conditions, where U_L is the load-side voltage with phase angle 0, E_i is the VSG voltage amplitude, δ_i is the VSG voltage phase angle to the load-side voltage phase angle (δi is the VSG power angle), I_i and I_L are the output current and load current of VSG respectively, Z_i=R_i+jX_i is the equivalent transmission impedance (sum of output impedance and line impedance), Z_L is the common load, and I_h is the current circulation between the two VSGs, where i =1, 2.

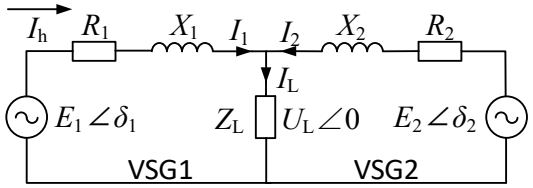

Fig. 4. Parallel equivalent circuit of two virtual synchronous generators

B. VSG power coupling analysis

Defining θ as the impedance angle of the transmission impedance Z_i, then:

$$\cos\theta = \frac{R_i}{Z_i}, \sin\theta = \frac{X_i}{Z_i} \tag{3}$$

The expressions for the active and reactive power output from the VSG are:

$$\begin{cases} P_i = (\dfrac{E_i U_L \cos\delta_i - U_L^2}{Z_i})\cos\theta + \dfrac{E_i U_L}{Z_i}\sin\delta_i \sin\theta \\ Q_i = (\dfrac{E_i U_L \cos\delta_i - U_L^2}{Z_i})\sin\theta - \dfrac{E_i U_L}{Z_i}\sin\delta_i \cos\theta \end{cases} \tag{4}$$

By substituting (3) into the above power expression, it is possible to get:

$$\begin{cases} P_i = \dfrac{(E_i U_L R_i \cos\delta_i - U_L^2 R_i + E_i U_L X_i \sin\delta_i)}{Z_i^2} \\ Q_i = \dfrac{(E_i U_L X_i \cos\delta_i - U_L^2 X_i - E_i U_L R_i \sin\delta_i)}{Z_i^2} \end{cases} \tag{5}$$

Taking the partial derivatives of P and Q with respect to E and δ, the expression of the influence of fluctuation on power is obtained:

$$\begin{cases} \dfrac{\partial P}{\partial \delta} = \dfrac{E U_L}{Z}\sin(\theta - \delta) \\ \dfrac{\partial P}{\partial E} = \dfrac{U_L}{Z}\cos(\theta - \delta) \\ \dfrac{\partial Q}{\partial \delta} = \dfrac{-E U_L}{Z}\cos(\theta - \delta) \\ \dfrac{\partial Q}{\partial E} = \dfrac{U_L}{Z}\sin(\theta - \delta) \end{cases} \tag{6}$$

It can be seen from (6) that both active and reactive power output by VSG are related to the phase amplitude of the output voltage and are affected by the transmission impedance. There is a certain coupling between active and reactive power, and the greater the resistive share of the transmission impedance, the smaller the impedance angle θ will be and the stronger the coupling between the powers will be. The coupling between powers is detrimental to the power distribution of the inverter parallel system and tends to cause power oscillations and generate current circulation.

Under low-voltage microgrid conditions, the key to achieving power decoupling is to ignore the resistive component of the transmission impedance so that it is strongly inductive when $Z_i \approx jX_i$ and the phase angle δ_i is small, taking the equivalent values $\sin\delta_i \approx \delta_i$ and $\cos\delta_i \approx 1$. The power expression can be simplified as:

$$\begin{cases} P_i = \dfrac{E_i U_L}{X_i}\delta_i \\ Q_i = \dfrac{(E_i - U_L)U_L}{X_i} \end{cases} \tag{7}$$

From (7), it can be obtained that when the equivalent transmission impedance is inductive, the active power is related to the voltage phase angle, the reactive power is related to the voltage magnitude difference, and the decoupling between the powers is achieved.

To achieve stable operation of a multi-VSG parallel system and allow the power to be distributed according to the set ratio, the parameters need to fulfil certain constraints [9]. The capacities of two VSGS are set as S1 and S2 respectively, and the capacity ratio is 1:N. In order to evenly divide the output power according to the capacity ratio, the parameter setting must meet the following requirements:

$$\frac{K_{\omega 1}}{K_{\omega 2}} = \frac{K_{q2}}{K_{q1}} = \frac{J_1}{J_2} = \frac{D_1}{D_2} = \frac{X_2}{X_1} = \frac{1}{N} \tag{8}$$

However, in practice, due to the location of the distributed power supply, the material and length of the transmission line, and other factors, there will be actual differences in line impedance. The transmission impedance will become resistive and result in power coupling if the line impedances do not meet the ratio of the specified capacity.

Figs. 2 and 3 show that the VSG active power loop has an integrator, the active power can be distributed according to the proportion of the active power-frequency modulation coefficient, and the line impedance has little influence on the active power distribution, while the reactive power loop does not contain an integrator. The reactive power distribution is less resilient and more susceptible to line impedance effects than the active power distribution. As a result, power distribution struggles to produce the desired results.

C. Analysis of current circulation characteristics

The output currents I_1 and I_2 of VSG in Fig. 4 are expressed as:

$$\begin{cases} I_1 = \dfrac{E_1\angle\delta_1 - U_L\angle 0}{R_1 + jX_1} = \dfrac{E_1\cos\delta_1 - U_L + jE_1\sin\delta_1}{R_1 + jX_1} \\ I_2 = \dfrac{E_2\angle\delta_2 - U_L\angle 0}{R_2 + jX_2} = \dfrac{E_2\cos\delta_2 - U_L + jE_2\sin\delta_2}{R_2 + jX_2} \end{cases} \tag{9}$$

Assume that two VSGs have equal transmission impedances and that both of them are inductive. Under this condition, $Z_1 = Z_2 \approx jX$, the circulating current I_h with the same capacity can be expressed as:

$$I_h = \frac{E_1\delta_1 - E_2\delta_2}{2X} - j\frac{E_1 - E_2}{2X} \tag{10}$$

From the expression for the circulating current, it is clear that to make the circulating current between the two VSGs as small as possible, it is necessary to control the phase and amplitude of the output voltage to be as identical as possible and to increase the equivalent transmission impedance.

IV. Dynamic Virtual Impedance Strategy Based on Fuzzy Control

A. Dynamic virtual impedance design

It is evident from the study in the preceding section that an imbalance in line impedance can affect a parallel system. The traditional virtual impedance strategy is designed to change the equivalent output impedance of the system by designing a fixed virtual impedance, but it ignores the effect of the line impedance. To compensate for the effects of line impedance differences, this paper designs a virtual impedance that can be dynamically adjusted with changes in output power. By adding a dynamic virtual impedance to make the equivalent impedance appear strongly inductive, the power coupling phenomenon caused by line impedance deviations can be improved to enhance power distribution accuracy.

The power coupling analysis predicts that as the load is altered, the power angle will change as well, resulting in some interaction between the active and reactive power. If the virtual impedance is not changed, the power coupling will intensify. Therefore, the main idea of dynamic virtual impedance is to adjust the impedance angle θ by estimating the amount of fluctuation of the power angle δ in real time in order to keep the impedance angle consistent for each line so as to change the magnitude of the virtual impedances R_v and L_v.

To analyze the effect of changes in work angle δ and impedance angle θ on power, the expressions for the variation of P and Q with θ and δ are obtained as follows:

$$\begin{cases} \Delta P = \left[\dfrac{U_L^2}{Z}\sin\theta - \dfrac{EU_L}{Z}\sin(\theta-\delta)\right]\Delta\theta \\ \quad + \dfrac{EU_L}{Z}\sin(\theta-\delta)\Delta\delta \\ \Delta Q = \left[\dfrac{-U_L^2}{Z}\cos\theta + \dfrac{EU_L}{Z}\cos(\theta-\delta)\right]\Delta\theta \\ \quad - \dfrac{EU_L}{Z}\cos(\theta-\delta)\Delta\delta \end{cases} \tag{11}$$

Taking into account the effect of line impedance, we expect the impedance angle of each line to remain the same before and after the change in power angle to keep the impedance ratio matching the capacity ratio. Then the equivalent impedance can be expressed as:

$$\begin{cases} Z_o\angle\theta_o + Z_v\angle\theta_v = Z\angle\theta \\ Z_o\angle\theta_o + Z_v^*\angle\theta_v^* = Z\angle(\theta^*+\delta) \end{cases} \tag{12}$$

Where, Z_o is the line impedance; θ_o is the line impedance angle; Z_v* is the post-change virtual impedance; θ_v* is the post-change virtual impedance angle; Z is the equivalent impedance; θ* is the post-change impedance angle.

To achieve complete decoupling of active and reactive power, the transmission impedance needs to be assumed to be close to purely inductive. As can be seen from (7), when the power angle changes, the active power of VSG changes with it, and if there is no coupling between the powers, the reactive power remains unchanged, Therefore, the impedance angle change can be obtained by ΔQ=0:

$$\Delta\theta = \frac{E\cos(\theta-\delta)}{E\cos(\theta-\delta) - U_L\cos\theta}\Delta\delta = m\Delta\delta \tag{13}$$

In the case where the equivalent impedance is inductive, the impedance angle θ is taken to be 90°, and the coefficient m is approximately equal to 1. If the change in impedance angle Δθv of the virtual impedance is used in place of the change in impedance angle, it is obtained from (13):

$$\Delta\theta_v \approx \Delta\theta \approx \Delta\delta \tag{14}$$

The crux of decoupling is to enhance the inductance of the output impedance and reduce the resistivity, but if the resistivity of the actual system disappears completely, the system will not operate stably [12], so $|R_v| \le |R|$ is designed, and eventually the virtual impedance expression is obtained after the power angle is changed as follows:

$$\begin{cases} R_v^* = \sin\delta\sqrt{R_o^2+X_o^2} - R_o \\ X_v^* = \cos\delta\sqrt{R_o^2+X_o^2} - X_o \end{cases} \tag{15}$$

B. Power angle monitoring based on fuzzy control

Analyzing the effect of power angle fluctuations on the output power is given by (1), (6), and (7):

$$\Delta P = \frac{\partial P}{\partial\delta}\Delta\delta = \frac{EU_L\sin\delta}{Z}\Delta\delta = K\Delta\delta \tag{16}$$

Considering the voltage amplitude E as a constant, the coefficient K is a function containing the power angle δ. The expression for K is:

$$K = f(\delta) = \frac{EU_L\sin\delta}{Z} \tag{17}$$

When the active power changes, the change in power angle $\Delta\delta$ and the coefficient K both change. Therefore, the relationship between the change in active power ΔP and the change in power angle $\Delta\delta$ is non-linear, so the fuzzy control algorithm is used to deal with the relationship between ΔP and $\Delta\delta$.

The fuzzy system mainly consists of a fuzzy controller and a control object, and its control process mainly contains: fuzzification, fuzzy inference, and clarification. The structure diagram of the two-dimensional fuzzy control system used in this paper is shown in Fig. 5. The fuzzy controller has two controlled objects, namely power deviation ΔP and power deviation change rate d(ΔP)/dt. The language variable E represents the input ΔP, EC represents the input d(ΔP)/dt, and U represents the output $\Delta\delta$.

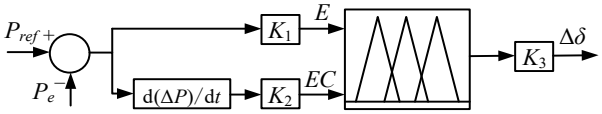

Fig. 5. Fuzzy control system structure diagram

Set the actual variation range as [-x, x], the discrete domain as [-n, -n+1,..., -1, 0, 1,..., n-1, n], and then the fuzzy quantization factor is:

$$K_i = \frac{n}{x} \tag{18}$$

In the MATLAB fuzzy logic toolbox, a standard (Mamdani) model fuzzy logic system is used with a triangular-type affiliation function (trimf) and a Gaussian-type affiliation function (gaussmf) for the input and output variables. The fuzzy domains of both input ΔP and d(ΔP)/dt are set to [-3, 3], and the corresponding sets of fuzzy linguistic values are T(E) = T(EC) = NB (negative large), NM (negative medium), NS (negative small), ZE (zero), PS (positive small), PM (positive medium), and PB (positive large); the fuzzy domain of output $\Delta\delta$ was set to [0, 1], and the corresponding set of fuzzy linguistic values remains unchanged. The input and output curves of the affiliation function are shown in Fig. 6.

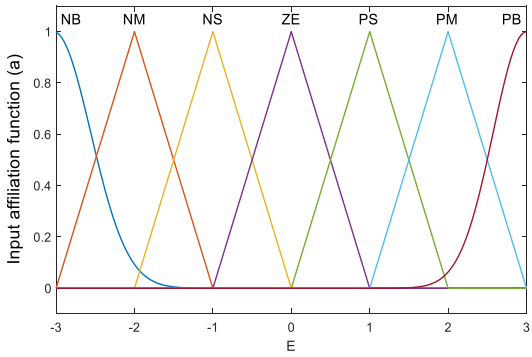

(a). Affiliation function of power deviation

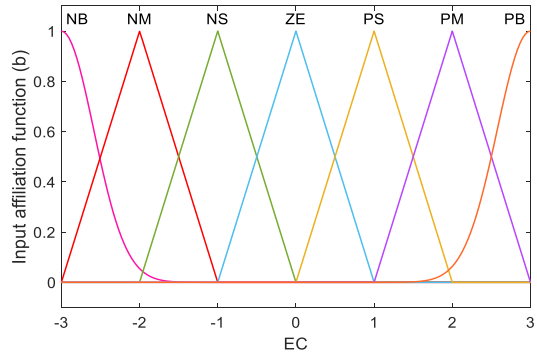

(b). Affiliation function of power deviation rate of change

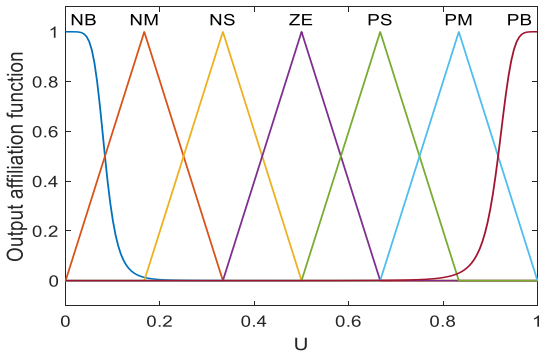

(c). Affiliation function of power angle variation

Fig. 6. Input/Output curves of affiliation function

Table I is the fuzzy control rule table adopted by the fuzzy controller, which contains 49 rules.

TABLE I
FUZZY CONTROL RULE

EC	E						
	NB	NM	NS	ZE	PS	PM	PB
NB	NB	NB	NB	NM	NS	PS	PS
NM	NB	NB	NM	NM	NS	PM	PM
NS	NB	NB	NM	NS	ZE	PM	PB
ZE	NB	NM	NS	NS	ZE	PM	PB
PS	NB	NM	NS	ZE	PS	PB	PB
PM	NM	NS	NS	ZE	PM	PB	PB
PB	NS	NS	NS	PS	PM	PB	PB

After the above fuzzy reasoning, the centroid is used to convert the fuzzy quantity into a precise quantity by sharpening it, and the system output characteristic surface diagram as shown in Fig. 7 is obtained.

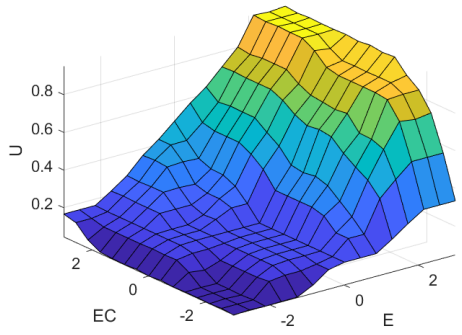

Fig. 7. System output characteristic surface diagram

V. SIMULATION ANALYSIS

In order to verify the effectiveness of the proposed improved virtual impedance strategy, a simulation model was built on the MATLAB/Simulink platform. Taking two VSG control systems in parallel as an example, the main parameters of the system are shown in Table II.

TABLE II
System Main Parameter Settings

Parameter	Value	Parameter	Value
Rated frequency (Hz)	50	Line resistance/R_1(Ω)	0.4
DC busbar voltage/U_{dc}(V)	800	Line resistance/R_2(Ω)	0.6
Filter inductance/L_f (mH)	3	Line reactance/L_1(mH)	2
Filter capacitors/C_f (μF)	30	Line reactance/L_2(mH)	3
Active power-frequency modulation coefficient/K_ω	0.04	Reactive power-voltage regulation coefficient/K_q	3e-4

A. Simulation verification of VSG with the same capacity under load surge conditions

Firstly, the power allocation effect of the improved dynamic virtual impedance decoupling strategy is verified when the two VSGs have the same capacity ratio and the line impedance is not average. Setting the capacity ratio at 1:1 and the line impedance at a ratio of 2:3, the total duration of the simulation is set at 1 s, starting operation with an active load of 6 kW and a reactive load of 3 kVar and adding the same size load at 0.5 s. Figs. 8 and 9 show the simulation results under the action of the conventional virtual impedance strategy and the dynamic virtual impedance strategy respectively.

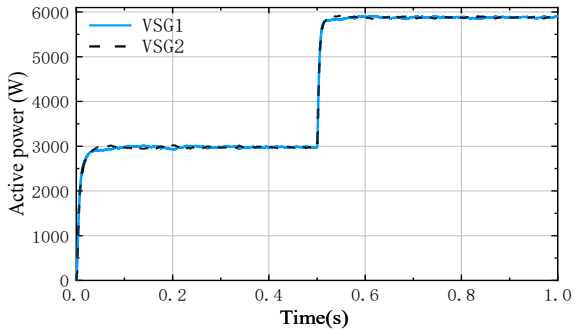

(a). Active power distribution results

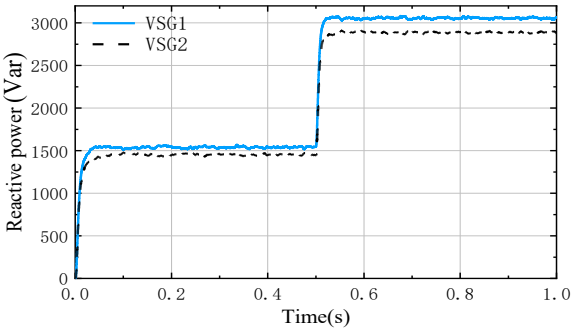

(b). Reactive power distribution results

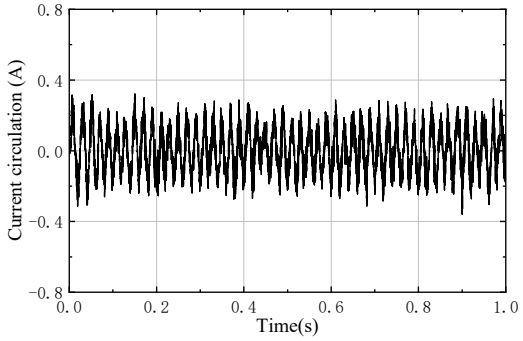

(c). VSG current circulation

Fig. 8. Traditional virtual impedance strategy

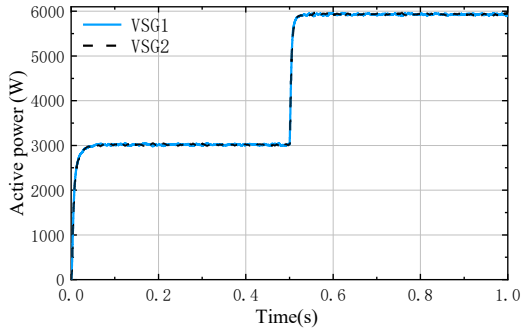

(a). Active power distribution results

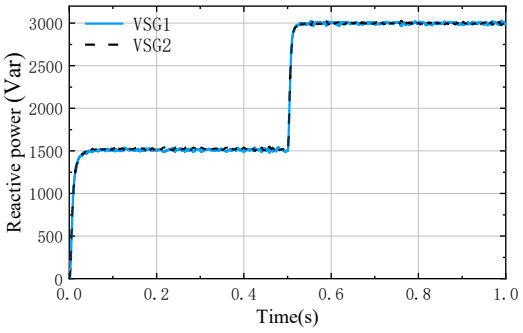

(b). Reactive power distribution results

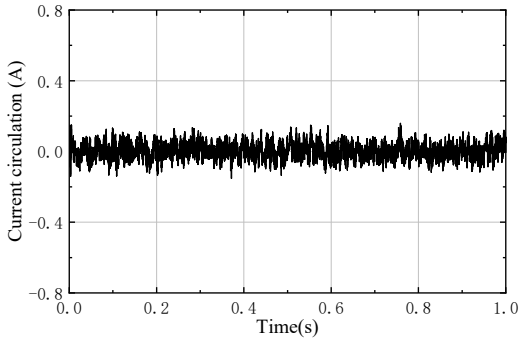

(c). VSG current circulation

Fig. 9. Improved dynamic virtual impedance strategy

As can be seen from Figs. 8 and 9, the traditional virtual impedance decoupling strategy does not address the impact of line impedance differences, reactive power fails to achieve equal distribution, and active power also has power oscillations during load switching due to the presence of coupling. When the improved dynamic virtual impedance strategy is adopted, the active and reactive power are equally distributed according to the 1:1 capacity ratio before and after the load surge. The fluctuation range of current circulation decreases from ±0.35A to ±0.15A, and the inhibition effect is obviously improved.

B. Simulation verification of VSG with different capacities under load surge conditions

To verify the effectiveness of the improved strategy for power decoupling when the VSG is set to different capacities and the load is suddenly increased, the line impedance ratio is kept unchanged, the capacity ratio is set to 2:1, both common active loads 1 and 2 are set to 6 kW and the reactive load is set to 3 kVar. The simulation duration is 1 s, load 1 is connected at the start of operation and load 2 is added at 0.5 s. Fig. 10 shows the simulation results under conventional virtual impedance regulation, and Fig. 11 shows the VSG simulation results under dynamic virtual impedance regulation.

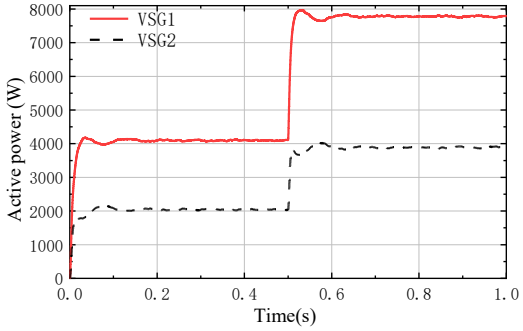

(a). Active power distribution results

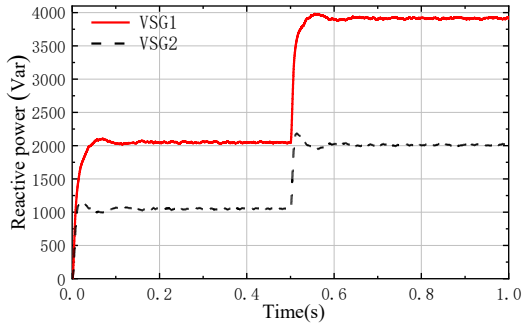

(b). Reactive power distribution results

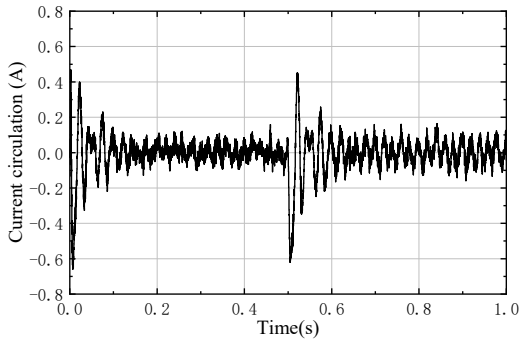

(c). VSG current circulation

Fig. 10 Traditional Virtual Impedance Strategy

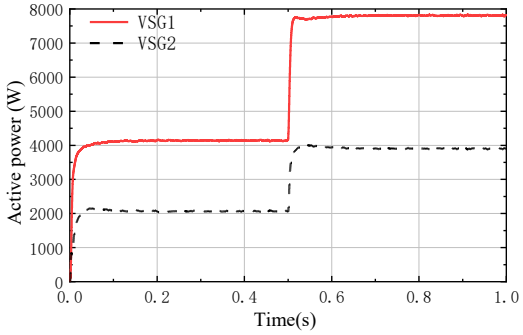

(a). Active power distribution results

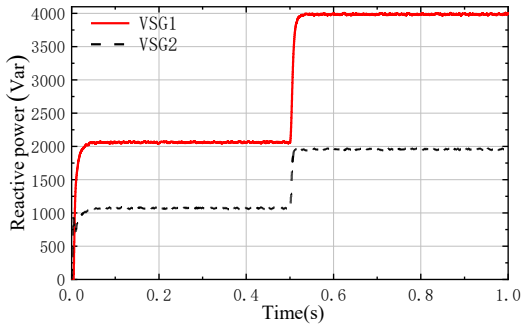

(b). Reactive power distribution results

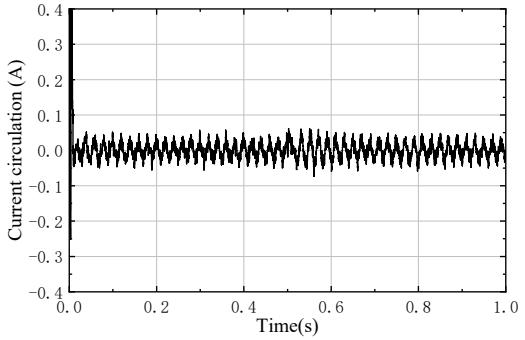

(c). VSG current circulation

Fig. 11. Improved dynamic virtual impedance strategy

From the comparison results of the two strategies, it can be seen that the traditional strategy is still affected by the line impedance, the coupling between active and reactive power exists, the power distribution is not accurate, the system overshoot is too large, the adjustment time is long, and the current circulation fluctuates within the range of ±0.2-±0.4A. As can be seen from Fig. 11, when the improved strategy is adopted, the power distribution of active and reactive power is evenly divided according to the capacity ratio of 2:1. When the load increases abruptly, the power does not fluctuate greatly and can still be evenly divided. In the steady state, the current circulation is smaller and the fluctuation range is reduced to ±0.05~±0.07A. The decoupling effect of active and reactive power is significantly more effective.

VI. Conclusion

In this paper, it proposes a power decoupling strategy based on dynamic virtual impedance. Firstly, it adopts a fuzzy algorithm to deal with the non-linear relationship between power fluctuation and power angle variation, and then estimates the power angle and uses the power angle fluctuation to adjust the virtual impedance so that the equivalent transmission impedance is strongly inductive, which solves the problem of power uneven distribution caused by the mismatch between line impedance and capacity ratio. Finally, the decoupling of power is realized. Compared with the traditional virtual impedance strategy, the proposed method has significantly improved the distribution accuracy, reduced regulation time, and suppressed current circulation, which greatly improves the stability of the inverter parallel system.

References

[1] K. M. Cheema, N. I. Chaudhary， M. F. Tahir，K. Mehmood， M. Mudassir, and M. Kamran, "Virtual synchronous generator: Modifications, stability assessment and future applications，" *Energy Reports*, vol. 8 (2022), pp. 1704–1717.

[2] Y. X. JIN, "Power Distribution Strategy of Parallel Inverter System Based on Virtual Synchronous Generator," *Harbin Institute of Technology*, 2020.

[3] B. Q. WANG, "Research on Control Strategy of Microgrid Inverter Based on Virtual Synchronous Generator," *Zhengzhou University*, 2021.

[4] Y. Li, F. Deng, R. Qi, and H. Lin, "Adaptive virtual impedance regulation strategy for reactive and harmonic power sharing among paralleled virtual synchronous generators," *International Journal of Electrical Power & Energy Systems*, 2022, 140: 108059.

[5] H. Chen, X. H. Yang, Y. F. Zhang, and Y. Liu, "Strategy of power decoupling for VSG based on virtual impedance of fuzzy control," *Electrical Measurement & Instrumentation*, 2020, 57(14): 135-141.

[6] X. F. Wan, Z. L. Zhan, and X H Ding, "Improved control strategy of multi-inverter parallel based on virtual synchronous generator," *Electric Machines and Control*, 2020, 24(02): 118-127.

[7] Z. S. Qu, Y. Y. Cai, H. Yang, N. B. Dong, R. X. Zhao, and J. F. Han, "Strategy of Power Decoupling Control for Virtual Synchronous Generator Based on Adaptive Virtual Impedances," *Automation of Electric Power Systems*, 2018, 42(17): 58-66.

[8] W. Dai, W. P. Qin, and C. G. Ren, "Adaptive Virtual Impedance Control Based on Decoupling Droop in Microgrid with Synchronous Generators," *Proceedings of the CSEE*, 2020, 40(14): 4486-4495+4728.

[9] C. X. Wen, Y. Z. Huang, and C. B. Hu, "Adaptive Control of Virtual Impedance in Parallel Operation of Virtual Synchronous Generator Interface Converter," *Transactions of China Electrotechnical Society*, 2020, 35(S2): 494-502.

[10] C. M. Yang, L. J. Sun, and M. Wu, "Improved VSG Control Method Based on Impedance Identification for Reactive Power Sharing in Parallel Inverter," *Control Engineering of China*, 2020, 27(01): 77-83.

[11] S. X. Cao and C. B. Wen, "Power sharing strategy of virtual synchronous generator multimachine parallel based on distributed consistency control," *Journal of Shanghai Dianji University*, 2021, 24(06): 311-317+324.

[12] H. Xu, C. Yu, C. Liu, Q. Wang, F. Liu and F. Li, "An Improved Virtual Capacitor Algorithm for Reactive Power Sharing in Multi-Paralleled Distributed Generators," *IEEE Transactions on Power Electronics*, vol. 34, no. 11, pp. 10786-10795, 2019.

[13] H. Xu, X. Zhang, F. Liu, R. Shi, C. Yu and R. Cao, "A Reactive Power Sharing Strategy of VSG Based on Virtual Capacitor Algorithm," *IEEE Transactions on Industrial Electronics*, vol. 64, no. 9, pp. 7520-7531, 2017.

[14] X. Liang, C. Andalib-Bin-Karim, W. Li, M. Mitolo, and M. N. S. K. Shabbir, "Adaptive Virtual Impedance-Based Reactive Power Sharing in Virtual Synchronous Generator Controlled Microgrids," *IEEE Transactions on Industry Applications*, vol. 57, no. 1, pp. 46-60, 2021.